CHEMISTRY & SUSTAINABILITY

CHEMSUSCHEM

ENERGY & MATERIALS

Accepted Article

Title: Sodium naphthalene-2,6-dicarboxylate: an Anode for Sodium Batteries

Authors: Joel M Cabañero, Vanessa Pereira Pimenta, Kieran Cannon, Russell Morris, and Anthony Robert Armstrong

To be cited as: *ChemSusChem* 10.1002/cssc.201901626

Link to VoR: http://dx.doi.org/10.1002/cssc.201901626

A Journal of

ChemPubSoc Europe

WILEY-VCH

www.chemsuschem.org

FULL PAPER

Sodium naphthalene-2,6-dicarboxylate: an Anode for Sodium Batteries

Joel M. Cabañero Jr,[a] Vanessa Pimenta,[a] Kieran C. Cannon,[a] Russell E. Morris[a,b] and A. Robert Armstrong*[a]

Abstract: The conjugated dicarboxylate, sodium naphthalene-2,6-dicarboxylate (Na_2NDC), has been prepared by a low energy consumption reflux method and its performance as a negative electrode for sodium-ion batteries evaluated in electrochemical cells. The structure of Na_2NDC was solved for the first time (monoclinic $P2_1/c$) from powder X-ray diffraction data and consists of π-stacked naphthalene units separated by sodium-oxygen layers. Through an appropriate choice of binder and conducting carbon additive Na_2NDC exhibits a reversible two electron sodium insertion at around 0.4 V vs. Na^+/Na with remarkably stable capacities of ca. 200 mA h g^{-1} at a rate of C/2 and good rate capability (~133 mA h g-1 at 5C). In parallel the high thermal stability of the material is demonstrated by HT-X-ray diffraction, the framework remaining intact to above 500 °C.

Introduction

The increasing demand for energy is one of the major challenges of the present century and has driven the search for new electrode materials for rechargeable battery applications. Lithium-ion batteries have been preferred to their sodium-ion counterparts by virtue of their higher energy density and operating voltages, leading to their domination of the portable electronics market and making them the best candidate for electric vehicles,[1] but concerns about lithium supply have encouraged the development of more sustainable sodium-ion batteries.[2-10] This rising interest in sodium-ion batteries has been driven by the greater and more uniform Earth abundance of sodium, compared with lithium, and resulting lower cost. Sodium-ion batteries could have a significant role in next-generation low-carbon energy technologies associated with the growing requirement for large scale batteries to store the electricity from solar cells, wind turbines and other renewable sources. The larger mass of sodium, compared with lithium, leads to a lower specific capacity, but this represents no disadvantage for static applications such as grid storage. In the case of lithium-ion batteries anode materials operating below around 0.5 V vs Li^+/Li require the use of copper as the current collector, thereby increasing cost, weight and environmental impact. One considerable advantage of sodium-ion batteries is the absence of an alloying reaction with aluminium which means that it can be used as a current collector regardless of voltage, providing an additional cost and environmental benefit.

Armand *et al.* were the first to demonstrate the potential application of conjugated dicarboxylates as anode materials for lithium-ion batteries.[11] These phases have the advantage that the raw materials can readily be obtained from green and sustainable sources such as the recycling of plastic bottles and biomass. By developing a procedure first reported by Kaduk,[12] they synthesized di-lithium terephthalate ($Li_2C_6H_4O_4$) and di-lithium *trans-trans*-muconate ($Li_2C_8H_4O_4$). The electrochemical performance of di-lithium *trans-trans*-muconate showed an overall reversible capacity corresponding to approximately 1 Li per formula unit at a potential of 1.4 V vs Li^+/Li, while the terephthalate salt exhibited a highly promising capacity corresponding to insertion/extraction of 2 Li at the lower voltage of 0.8 V vs Li^+/Li. The latter corresponds to a reversible capacity of ~ 300 $mAhg^{-1}$, with 234 $mAhg^{-1}$ retained after 50 cycles. As a consequence of this study several other conjugated dicarboxylates have been described as anodes for lithium-ion batteries. Ogihara *et al.* reported excellent performance for lithium 2,6-naphthalenedicarboxylate ($(2,6\text{-Naph(COOLi)}_2)$).[13,14] The discharge capacity on the first cycle corresponded to 3 Li^+ per molecule with a reversible capacity of 2 Li^+ and good capacity retention. The authors coined the term intercalated metal-organic framework or iMOF for the material, which had previously been described as UL-MOF-1.[15] The low discharge voltage of 0.8 V vs Li^+/Li, small cell polarization and very low volume change of 0.33% make lithium 2,6-naphthalenedicarboxylate a promising negative electrode for high-voltage Li-ion batteries. The material also showed excellent thermal stability; up to 527°C under an Ar atmosphere.[14] Several other conjugated dicarboxylates such as lithium dihydroxyterephthalate have also shown promising performance as anode materials for lithium-ion batteries.[16,17]

One of the primary challenges in the development and commercial realisation of sodium-ion batteries is to find a suitable negative electrode. Whilst graphite has proved to be a very successful anode material for lithium-ion batteries, by contrast there is negligible sodium intercalation between the graphene sheets for most electrolyte systems.[18,19] A number of other forms of carbon have been investigated, however, and show promise. Amorphous hard carbon currently represents the best option for a working negative electrode, though it shows significant irreversible capacity on the first cycle.[8,20] Several conjugated dicarboxylates have also been evaluated as anodes for sodium-ion batteries including sodium terephthalate (sodium benzene-1,4-dicarboxylate), sodium 4,4'-biphenyldicarboxylate and sodium dihydroxyterephthalate, all with operating potentials of ~ 0.5 V vs Na^+/Na.[21-25] While these materials show reasonable capacities and attractive sodium insertion potentials, the rate performance is typically rather poor. Sodium 4,4'-biphenyldicarboxylate has demonstrated good rate performance,

[a] Joel M. Cabañero Jr, Dr Vanessa Pimenta, Kieran C. Cannon, Prof Russell E. Morris and Dr A. Robert Armstrong*
School of Chemistry
East Chem, University of St Andrews
North Haugh, St Andrews, Fife, KY16 9ST, United Kingdom
E-mail: ara@st-andrews.ac.uk

[b] Prof Russell E Morris
Department of Physical and Macromolecular Chemistry
Faculty of Sciences, Charles University
Hlavova 8, 128 43 Prague 2, Czech Republic

Supporting information for this article is given via a link at the end of the document.((Please delete this text if not appropriate))

albeit with only 57% active material in the electrode formulation.[24] Further new materials have recently been reported including disodium pyridine-2,5-dicarboxylate and sodium 2,6-naphthalene dicarboxylate.[26-28] Further examples are described in a recent review by Zhao et al.[29]

Na_2NDC has recently been highlighted as anode material by Deng *et al.*. The authors describe the synthesis of a graphene-wrapped nanocomposite displaying 118 mA h g^{-1} at 5C and 88 mA h g^{-1} at 10C.[27] Such performance is however enhanced by the synergetic presence of graphene sheets around Na_2NDC. More recently Medabalmi *et al.* reported that Na_2NDC at a rate of C/5, shows 145 mA h g^{-1} with 70% retention after 70 cycles and 85 mA h g^{-1} at 2.5C.[28] These results are already quite promising, however the electrochemical performance can still be improved without resorting to the complexity of wrapping with graphene

Herein we report a detailed study of sodium naphthalene-2,6-dicarboxylate (Na_2NDC). The crystal structure was determined for the first time (*ab initio* from powder diffraction data) and the framework robustness was highlighted by HT-XRD. The electrochemical performance was explored and with the appropriate choice of carbon additive and binder resulted in a remarkable electrochemical performance up to rates of 5C without the need to form a nanocomposite, with the low rate capacity exceeding 200 mA h g^{-1} and excellent cycling stability.

Results and Discussion

Structural characterization

Sodium naphthalene-2,6-dicarboxylate (Na_2NDC) was synthesised as described in the experimental section. The acid–base reaction of naphthalene-2,6-dicarboxylic acid (NDCA) with sodium hydroxide was verified by Fourier transform infrared (FT-IR) spectroscopy. As shown in **Figure 1** the spectrum of naphthalene-2,6-dicarboxylic acid (NDCA) shows a broad peak in the range 3250 – 2000 cm^{-1}, characteristic of carboxylic acids and arising from strong hydrogen bonding. This broad peak is absent from the IR spectrum of Na_2NDC which confirms the loss of the -OH functional group in the product and successful salt formation. The spectrum for NDCA also shows an intense carbonyl stretch at 1672 cm^{-1} and O–H bending vibrations from the carboxylic acid (COOH) groups at around 900 cm^{-1}. The formation of sodium naphthalene-2,6-dicarboxylate (Na_2NDC) via complete deprotonation by NaOH leads to a shift in the carbonyl stretching vibration of the carboxylate groups - a split into two bands at 1557 cm^{-1} and 1395 cm^{-1} respectively, which were assigned to asymmetric and symmetric stretching vibrations, respectively. Moreover, the characteristic O–H bending vibrations for the carboxylic acid groups, located around 900 cm^{-1}, disappeared. These values are in excellent agreement with those reported previously.[27] The chemical structure was confirmed using ^{1}H and ^{13}C DEPTQ NMR spectroscopy with D_2O as the solvent. The solvent exchanges readily with the protons of the carboxylic acid group; hence the NMR spectra of the acids and the salts were indistinguishable. Thus NMR alone was not a definitive tool for determining the structure and purity of the product since the presence of the excess ligand and/or monosodium compounds cannot be excluded. However, when NMR results are combined with FTIR and elemental analysis data, the structure could be elucidated (fig. S1). Elemental analysis results revealed high purity of the product with values of 55.29 % C, 2.29% H; compared to theoretical values of 55.40% C, 2.33% H.

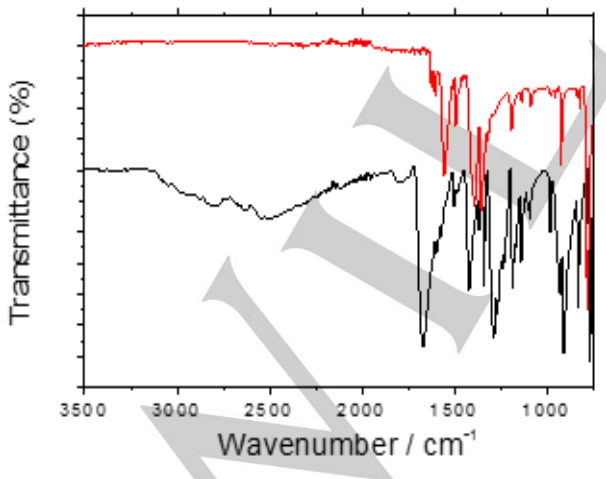

Figure 1. Infra-red spectra for sodium naphthalene-2,6-dicarboxylate (red line) and naphthalene-2,6-dicarboxylic acid (black line).

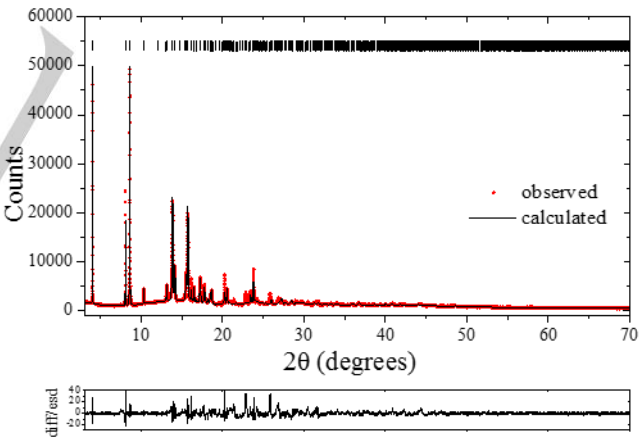

Figure 2. Fitted synchrotron X-ray diffraction pattern for Na_2NDC; the red dots represent the observed data and the solid line the calculated pattern; the lower line is the difference/esd. Tick marks represent the allowed reflections.

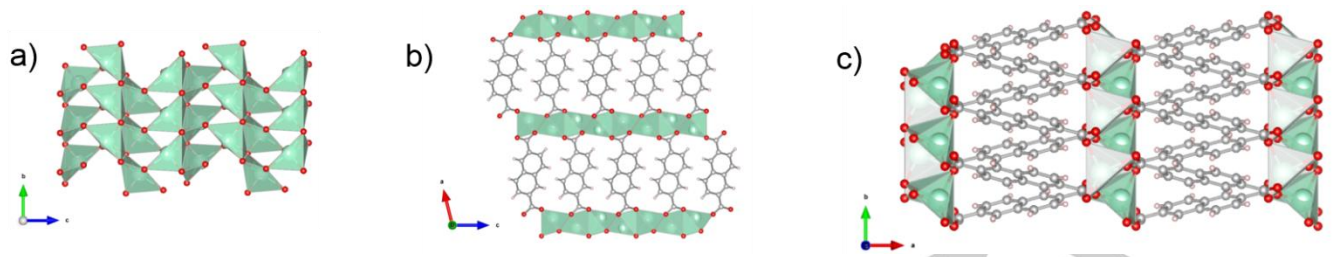

Figure 3. Schematic representation of the crystal structure of Na_2NDC: bc plan showing the sodium layers (a); stacking of the inorganic layers with deprotonated naphthalene rings along the [010] direction (b); 3D framework with small 1D cavities (c).

A powder X-ray diffraction pattern for Na_2NDC is shown in fig. S2. The pattern could be indexed on the basis of a monoclinic unit cell, space group $P2_1/c$, with approximate cell parameters a = 12.1, b = 3.6, c = 11.36 Å, β = 103.8°. A profile fit to the synchrotron X-ray diffraction data is shown in **Figure 2** and refined structural parameters are presented in Table S1. The π-stacking of the aromatic rings together with the rigid naphthalene structural unit enabled the crystal structure to be solved ab initio from powder diffraction data. This was achieved by analogy with the previously reported structure of potassium terephthalate.[12] Potassium terephthalate exhibits a generally similar set of unit cell parameters with analogous π-stacking of the aromatic rings (Fig.S3). In the case of Na_2NDC the additional limitations of the rigid molecular structure meant that the C-C bond at the junction of the fused benzene rings could be placed at the inversion centre of the unit cell. The structure was then refined using Topas Academic applying constraints to both bond lengths and angles.[30,31] Numerous other naphthalene derivatives crystallise in the monoclinic space group $P2_1/c$, in particular alkali based Li_2NDC, alkaline earth $Ca_2(OH)_2NDC$[32] or even 3d metal based frameworks such as $Zn_2(OH)_2NDC$[33] and $(V^{IV}O)_2(OH)_2NDC$ ($P2_1/n$).[34] Interestingly, sodium biphenyldicarboxylate (Na_2BPDC) also adopts the same type of structure.[24] The framework of Na_2NDC is built up from successive sodium layers separated by aromatic bridging units. The sodium ions show a rather irregular coordination environment, being penta-coordinated with Na-O bonds with a range of bond lengths from 1.78 – 3.08 Å. Sodium atoms occupy one independent crystallographic position and are associated in Na_2O_8 dimers through a sharing edge. Each dimer is connected to the adjacent also by two shared edges, forming $_\infty[Na_2O_7]$ chains. The chains alternate in opposite direction along b and are connected by four sharing corners (**Figure 3** a). The layered inorganic sub-units are stacked with deprotonated naphthalene rings along the [010] direction (**Figure 3** b) and the naphthalene rings are separated by 3.62 Å. The framework is three-dimensional with small cavities (**Figure 3** c). In order to investigate the porosity of the network, N_2 and CO_2 adsorption measurements were performed, however Na_2NDC did not show significant adsorption properties (Fig. S4).

A key feature of organic dicarboxylate anode materials is their unusually high thermal stability. In order to examine the thermal stability of Na_2NDC, thermogravimetric analysis (TGA) and temperature dependent X-ray diffraction were carried out (HT-XRD). As shown in **Figure 4** a, no significant weight loss is observed in the thermogram until around 500 °C, indicating retention of the framework. This excellent thermal stability is due to the efficient π-stacking interaction between adjacent naphthalene rings, as previously observed for the lithium

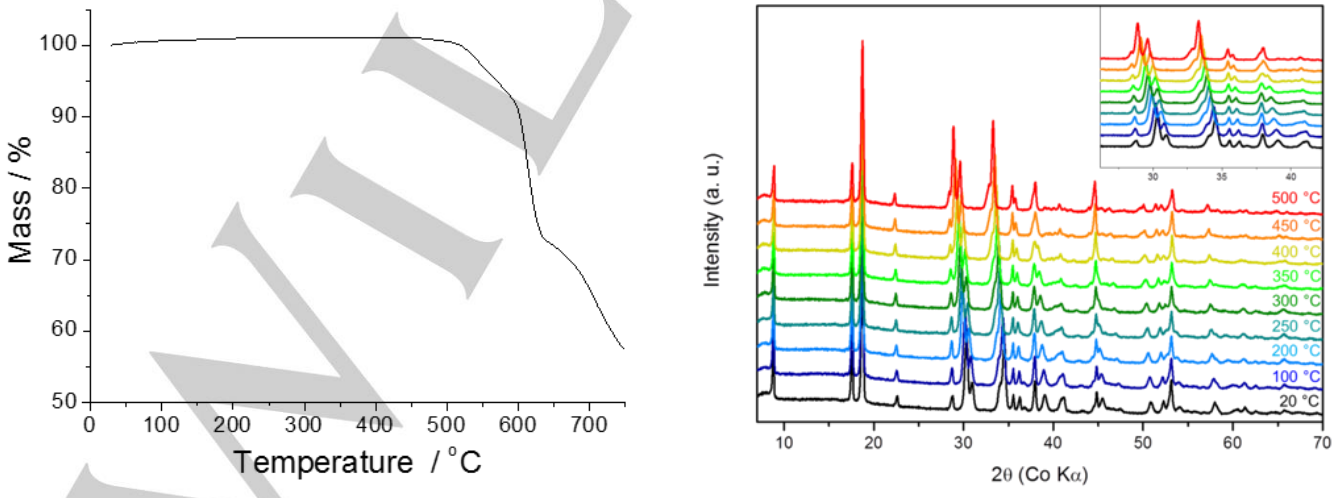

Figure 4. TGA trace for Na_2NDC under flowing argon at a heating rate of 2 °C per minute (a); HT-XRD of Na2NDC from RT to 500 °C under flowing helium at a heating rate of 2 °C per minute (b).

analogue.[14] **Figure 4** b shows the evolution of the X-ray pattern upon heating. The HT-XRD studies confirm the stability of the framework. Upon heating, a shift of the Bragg peaks at $2\theta = 30.5^{o}$ and 34.8^{o} towards lower angles indicates an evolution of the cell parameters. All patterns were refined using Le Bail fitting method, showing that upon heating the network becomes distorted, with a simultaneous increase of *b* parameter and unit cell volume, while β decreases and *a* and *b* stay more-or-less constant (Fig. S5). The distortion of the framework is fully reversible and all Bragg peaks shift to their initial position once the sample is cooled to room temperature. The X-ray powder diffractograms are shown in Fig. S6.

Electrochemical characterisation

The electrochemical performance of Na_2NDC was evaluated using coin cells with sodium metal as the negative electrode. Initial studies were performed using Super P carbon as the conducting additive with Kynar 2801 (a co-polymer based on PVDF) as the binder. Figure S7 shows the voltage profile of the first five cycles of the material at a rate of 0.1C (C rate defined as 200 mA g^{-1}), while **Figure 5** shows a cyclic voltammogram for the first 5 cycles at a sweep rate of 0.1 mV s^{-1}.

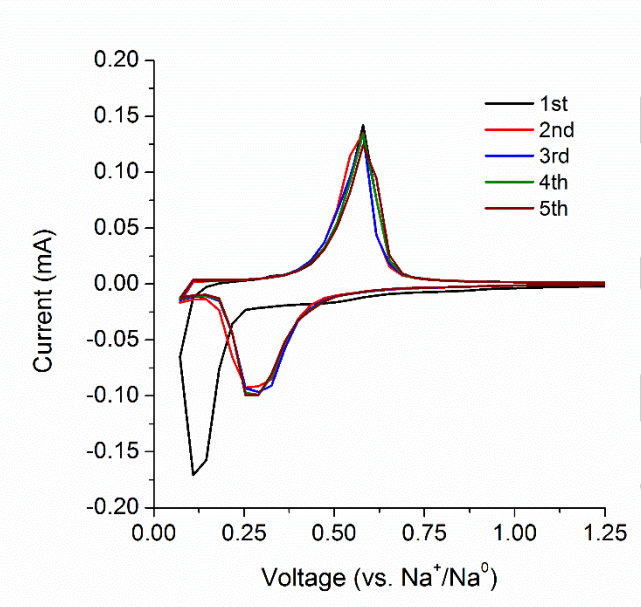

Figure 5. Cyclic voltammograms at a scan rate of 0.1 mV s^{-1} for Na_2NDC.

In common with similar sodium materials a large irreversible capacity is observed on the first cycle. This arises from two sources - the formation of solid electrolyte interphase (SEI) layer[35] and irreversible capacity from the conductive carbon additive. Compared to the already reported Li_2NDC compound[13], Na_2NDC shows a more significant irreversible capacity on the first cycle since the SEI formation mechanism in Na-ion batteries differs from that of Li systems. The SEI thickness in both LIBs and SIBs ranges from 10 to 100 nm.[36] However the main difference remains in the composition of the solid electrolyte interphase. In LIBs

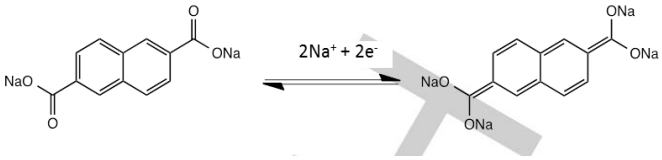

Equation 1. Proposed reaction scheme for sodium insertion and extraction in sodium naphthalene-2,6-dicarboxylate.

numerous organic and inorganic species make up the SEI. In SIBs both classes of compound are also present, however the presence of inorganic compounds is greater than the organic derivatives (both produced by the electrolyte and binder decomposition)[36,37] and the organic species are mainly distributed near the surface while the interior of the SEI is mainly composed of inorganic species.[38]

After taking the capacity contribution of the conductive carbon into account, the second discharge capacity is equivalent to approximately 2 Na^+, which corresponds to the theoretical capacity of Na_2NDC, according to the proposed reaction scheme shown in **Equation 1**.

On succeeding cycles the capacity remains at this value, providing confirmation that the discharge and charge processes of Na_2NDC involve a one-step two-electron reversible redox process as shown in Equation 1. The first discharge potential of 0.22 V vs. Na^+/Na is markedly lower than the second and subsequent discharges (0.38 V vs. Na^+/Na), whilst the charging potential remains at around 0.50 V. Similar, albeit less pronounced, behaviour was observed for the lithium analogue where a difference of 40 mV was observed between first and subsequent discharges. The raising of the voltage plateau from the first discharge process to the subsequent discharge processes of Li_2NDC is associated with the decrease in *IV* resistance after the initial Li intercalation.[13]

In order to investigate the phenomenon electrochemical impedance spectroscopy (EIS) was carried out at various states of charge.

Figure 6a shows the EIS Nyquist plots of the cell as-prepared (at OCV), at the end of the first discharge and after first and second charge. Bode plots can be found in fig. S7. As the measurements were performed in a two electrode half-cell, the EIS spectra includes the overall cell resistance. However, it can be assumed that the anode contribution remains constant since the ohmic resistance is similar in all cycles. For the as-prepared cell, the impedance is very high, the spectrum showing a complex shape with the overlapping of several features. Upon cycling the system becomes more conductive as evident from the decreased impedance (Figure 6b). After the first discharge, the high frequency (HF) semicircle corresponding to the SEI appears at ~25 kHz, which is more pronounced for the charged samples (Figure 6c,d), which explains the initial capacity loss due to the SEI formation. Furthermore, the mid-frequency semicircle (at ~60 Hz) corresponding to the charge transfer process at the SEI/electrode interface can be distinguished, along with the low-frequency Warburg tail[39], corresponding to the sodium diffusion in

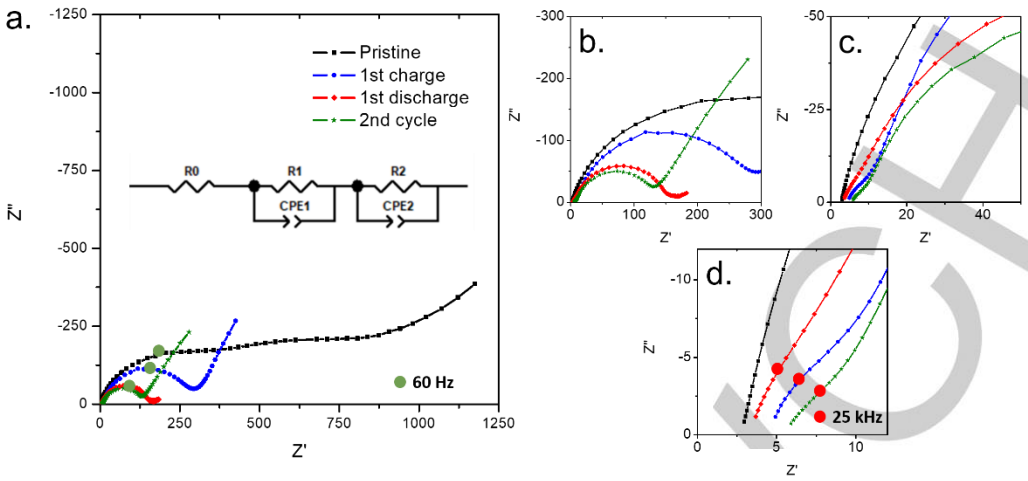

Figure 6. Impedance spectra for Na_2NDC at various states of charge (black – as-prepared electrode; red – after first discharge; blue – after one cycle; green – after two cycles)(a). High frequency regions of the spectra (b,c,d).

the electrode material. In subsequent cycling the R_{SEI} and R_{ct} remain in the same range, slightly increasing at the 1st charge but decreasing again after the 2nd full change (Table S2). As charge transfer resistance provides information about the kinetics of the Na insertion/disinsertion process, it can be said that in Na insertion step the low R_{CT} reveals an enhanced electron transfer, while in the Na disinsertion step the R_{CT} increases again, meaning a process with lower kinetics. After two cycles R_{CT} decreases again, suggesting that after the SEI formation the kinetics of the Na insertion is faster than at the 1st cycle. Although *ex-situ* powder X-ray diffraction patterns were recorded at different states of charge (fig. S8), it was not possible to refine the parameters and shed light to the sodium insertion mechanism. Nevertheless, it is clear from the patterns that the structure remains stable and reveal a highly reversible sodium insertion process with only small structural changes at the end of discharge. Compared to the Li compound, where a mixed electronic and ionic conductivity mechanism is highlighted[40], one cannot clearly indicate if the nature of the sodium intercalation mechanism is comparable. Further investigations in a three electrode cell, as well as pellet measurements at different temperatures will help to unravel the Na insertion mechanism and the activation energy. It is nonetheless possible to consider that among the three electron conduction hopping path demonstrated for the Li compound[40], Na_2NDC would show at least two similar hopping paths, since the π- stacking of the aromatic cycles is oriented in a similar way to Li_2NDC and the basal packing of sodium layers is ensured.

Whilst electrodes prepared with Super P carbon and PVDF-based binders showed high initial capacities (fig. S9), the long-term cycling stability was unsatisfactory (fig. S10). As a result, changes were made to both the conducting carbon additive and the binder. Use of carboxymethyl cellulose (CMC) as binder was found to result in enhanced cycling stability and improved rate capability, perhaps as a result of solubility of the electrode material in the deionized water used to prepare the slurry ensuring intimate mixing of the constituents. The use of CMC as a binder instead of PVDF has also been reported for the lithium equivalent.[41] The enhancement of the cycling performance can be explained by the amphiphilic character of CMC chains, where the carboxylate groups on the outside of the polymer chain have a hydrophilic character and the main chain has rather a hydrophobic character. Due to this amphiphilic character, the outside carboxylic groups interact with Na2NDC particles while the hydrophobic part with the conductive carbon additive. The Na_2NDC slurry had a dark black colour, meaning a homogeneous dispersion and a full coating of the white Na_2NDC particles as described for the Li_2NDC.[41] This full coating will therefore improve the electronic conductivity of the electrode. Cycling performance enhancement related to the use of CMC binder has also been reported in Na-ion batteries.[42] Compared to PVDF, the SEI formed when CMC is used has a smoother and more homogeneous surface, showing how binder degradation (PVDF fluorine content can contribute to the formation of insulating NaF) can also play a key role in SEI formation and consequently a long-term cycling stability.[37]

Cycling performance for electrodes containing 60% active material: 30% Super P carbon: 10% CMC at a variety of rates from 0.1C up to 1C is shown in fig. S11. This represents a performance enhancement compared with the results reported by Medabalmi *et al.* using PVDF as binder.[28]

In order to reduce the overall carbon content of the electrodes, partial replacement of Super P carbon with the higher surface area Ketjenblack carbon was investigated. This resulted in a further enhancement in the performance, especially at higher cycling rates.

The cycling performance of Na_2NDC with an electrode composition consisting of 65% active material: 10% Super P: 15% Ketjenblack: 10% CMC at rates of 100 mA g^{-1} (C/2) and 400 mA g^{-1} (2C) is shown in **Figure 7**.

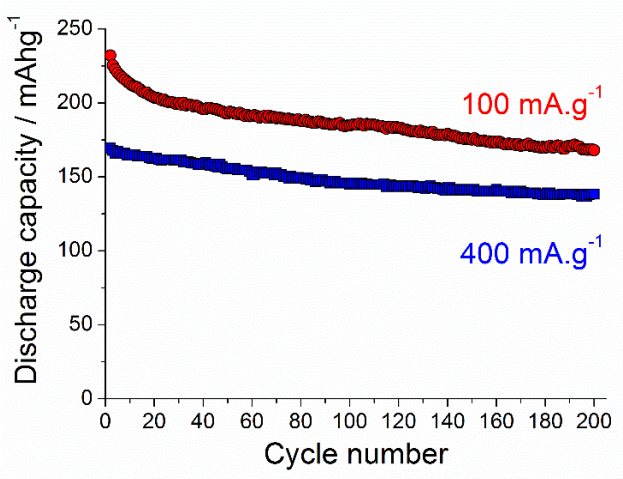

Figure 7. Cycling data for Na_2NDC obtained between 0.05 and 2.0 V vs. Na+/Na at 100 mA g^{-1} (C/2, red circles) and 400 mA g^{-1} (2C), blue squares).

An initial capacity of around 230 mA h g^{-1} was observed at the lower cycling rate and, after dropping over the first few cycles, this stabilizes at around 200 mA h g^{-1}. The initial capacity exceeds the theoretical value corresponding to the insertion of two sodium ions (208 mA h g^{-1}) as a result of a small contribution from the conducting carbon additive. In order to quantify this contribution, cells were fabricated with electrodes having the composition 36% Super P: 54% Ketjenblack: 10% CMC. These were then cycled under the same conditions. Load curves for these carbon electrodes from the 20th cycle, the point at which the capacity stabilizes, are shown in fig. S12 and reveal a contribution to the overall capacity corresponding to approximately 15 mA h g^{-1}. This value was higher for the first few cycles.

Very stable cycling was obtained for Na_2NDC even at the higher rate of 2C, with excellent capacity retention (99.92% per cycle) up to 200 charge-discharge cycles. Further evaluation of the rate performance was carried out by cycling for 10 cycles at

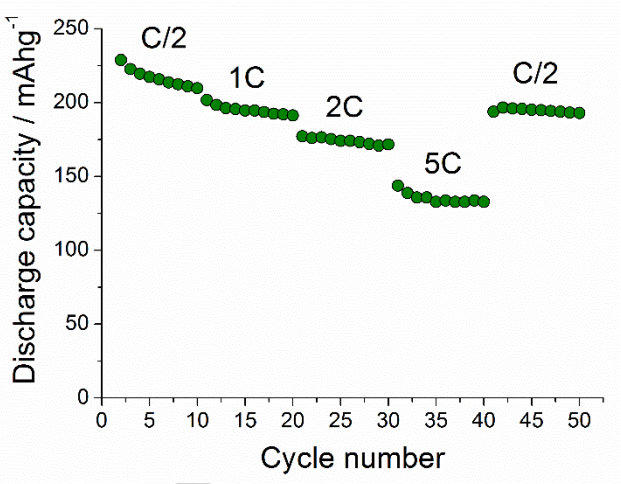

Figure 8. Rate performance for Na_2NDC obtained between 0.05 and 2.0 V vs. Na^+/Na at various rates and at room temperature. The data were recorded for a single cell, and the applied current was varied every 10 cycles. Rates are indicated on top of each set of data.

progressively increasing rates from C/2 (100 mA g^{-1}) up to 5C (1000 mA g^{-1}) before returning to C/2, as shown in **Figure 8**. High capacities are maintained up to a rate of 5C and on reducing the cycling rate to C/2 the capacity recovers to around 200 mA h g^{-1}.

Conclusions

Sodium naphthalene-2,6-dicarboxylate (Na_2NDC) has been prepared by a straightforward low-cost route, characterized using a range of techniques including PXRD, IR and TGA. The structure, determined ab initio from synchrotron powder X-ray diffraction data, consists of π-stacked naphthalene units which form layers along the [010] direction. This confers high thermal stability to above 500 °C.

The behaviour of Na_2NDC as an anode material in sodium-ion batteries has been studied. With appropriate choice of binder and conducting carbon additive Na_2NDC exhibits a reversible two electron sodium insertion at around 0.4 V vs. Na^+/Na and delivers stable high capacities of ca. 200 mA h g^{-1} at a rate of C/2 and good rate capability (~133 mA h g^{-1} at 5C).

Experimental Section

Synthesis of sodium naphthalene dicarboxylate (Na_2NDC): The synthesis of Na_2NDC was modified from that employed by Ogihara et al.[13] for the preparation of lithium naphthalene-2,6-dicarboxylate (Li_2NDC). Sodium hydroxide (0.5291g, 13.23 mmol) (as pre-dissolved in 100 ml methanol and naphthalene-2,6-dicarboxylic acid (NDCA) (1.0 g, 4.63 mmol) was rapidly added to the solution at room temperature while stirring. Formation of a white precipitate was observed within 20 minutes. The resulting suspension was then stirred under reflux conditions at 353 K for 24 h. The hot solution was vacuum filtered, washed twice with methanol and dried under vacuum at 413 K for 12 h.

Structural characterisation. In this study, the diffraction measurements were carried out on capillary samples (0.5mm) using a Stoe STADI/P diffractometer in Debye-Scherrer mode, using Cu $K\alpha_1$ radiation (λ = 1.54056 Å) and a position sensitive detector. Synchrotron X-ray diffraction data were obtained on capillaries using the I11 diffractometer at the Diamond Light Source, UK (λ = 0.825848(10) Å). Ex-situ powder XRD was performed in order to confirm the structural stability upon cycling. Pristine Na_2NDC was hand ground with Super C65 carbon and powders were collected after the 1st discharge and after one complete cycle. The cells were disassembled in an Ar-filled glovebox, and the powders washed with propylene carbonate and dried under vacuum overnight. The obtained powder was then transferred to capillaries for diffraction measurements. High-temperature X-ray thermodiffraction was carried out under helium flow from RT to 500°C in an Anton Paar XRK 900 high temperature furnace using a Panalytical X'Pert Pro diffractometer (Co K_α radiation).

Infrared spectroscopy was used as a tool for differentiating the starting material from the product. A Shimadzu IR affinity-1 Fourier Transform infrared spectrophotometer in attenuated total reflectance (ATR) mode was employed in this study and the samples were scanned in the range 600 - 3800 cm^{-1}.

Solution-phase ^1H and ^{13}C NMR were used to elucidate the chemical structure of the synthesized compounds. 13C NMR spectra editing was performed with DEPTQ (Distortionless Enhancement by Polarisation Transfer with retention of Quaternaries) in order to facilitate easier structure elucidation as the non-protonated carbons in the sample appear as a peak with a sign similar to that of CH_2 groups. All the samples were first dissolved in a deuterated solvent containing trimethylsilane (TMS) as an internal reference and were then measured on a 400 MHz Bruker Avance III spectrometer. ^1H NMR was performed at 400 MHz while ^{13}C NMR was performed at 100 MHz.

In this study, the elemental (CHN) analysis results were obtained using the service of London Metropolitan University, United Kingdom (S. Boyer). In order to probe the thermal stability of the material thermogravimetric analysis (TGA) was performed on a TA Instruments NETZSCH TG 209 instrument with simultaneous TGA/DTA furnace. Samples were heated from 30 °C at a rate of 2 °C/min to a maximum temperature of 750 °C under flowing argon.

Electrochemical characterisation: In the initial studies the working electrodes were made by mixing the active material (Na_2NDC), conductive carbon (Super P) and Kynar 2801 (a co-polymer based on PVDF) as binder in N-methyl-2-pyrrolidone. The slurry was then cast on aluminium foil using a doctor blade and dried overnight. Subsequent studies used carboxymethyl cellulose (CMC) as the binder and the slurry was mixed in deionized water. Ketjenblack was used as an alternative carbon source to Super P. Several active material/conductive carbon/CMC mass ratios were investigated including 60: 30 (Super P): 10 and 65: 10 (Super P): 15 (Ketjenblack): 10. The approximate active mass loading per disc was 2.5 mg cm^{-2}. Electrodes were incorporated into coin cells (CR2325 type, NRC Canada) with a sodium metal counter electrode, and with an electrolyte solution composed of 1M $NaClO_4$ in propylene carbonate (PC) containing 3% (wt) of fluoroethylene carbonate (FEC) additive. The cells were assembled in an argon-filled glove box (MBraun) with moisture content and oxygen level below 1 ppm. Electrochemical measurements were carried out at room temperature using a Biologic MacPile II system.

Electrochemical impedance spectroscopy (EIS) measurements were conducted on coin cells. Data were collected using a Solartron 1255 frequency response analyser coupled with Solartron 1287 electrochemical interface. A perturbation voltage of 10 mV, together with a frequency range of 0.1 Hz to 0.1 MHz, was employed. EIS was measured for the pristine sample, after the 1st discharge, 1st charge and two complete cycles.

Acknowledgements

We thank the EPSRC (EP/K025112/1) and the Leverhulme Trust (RPG-2016-323) for funding and Diamond Light Source for rapid access to synchrotron radiation facilities. We thank Dr. Paul A. Connor (School of Chemistry, University of St. Andrews) for assistance with EIS measurements, Sujoy Saha (Collège de France) for the EIS fitting and Dr. Philip Landon for the HT-XRD measurements.

Keywords: Batteries • Na-ion • organic redox • anodes • MOFs

[1] D. Larcher, J-M. Tarascon, *Nature Chem*., **2015**, *1*, 19.
[2] S-W. Kim, D-H. Seo, X. Ma, G. Ceder and K. Kang, *Adv. Energy Mater.*, 2012, **2**, 710.
[3] B. L. Ellis, L. F. Nazar, *Current Opinion in Solid State and Materials Science*, 2012, **16**, 168.
[4] V. Palomares, P. Serras, I. Villaluenga, K. B. Hueso, J. C. González, T. Rojo, T. *Energy Environ. Sci*., **2012**, 5, 5884.
[5] V. Palomares, M. C. Cabanas, E. C. Martínez, M. H. Han, T. Rojo, *Energy Environ. Sci*., **2013**, 6, 2312.
[6] H. Pan, Y.-S. Hu, L. Chen, *Energy Environ. Sci*., **2013**, 6, 2338.
[7] M. D. Slater, D. Kim, E. Lee, C. S. Johnson, *Adv. Funct. Mater*., **2013**, 23, 947.
[8] A. Ponrouch, E. Marchante, M. Courty, J.-M. Tarascon, M. R. Palacin, *Energy Environ. Sci*., **2012**, 5, 8572.
[9] K. Kubota, S. Komaba, *J. Electrochem. Soc.*, **2015**, 162, A2538.
[10] J.-Y. Hwang, S.-T. Myung, Y.-K. Sun, *Chem.Soc. Rev.*, **2017**, 46, 3529.
[11] M. Armand, S. Grugeon, H. Vezin, S. Laruelle, P. Ribière, P. Poizot, J.-M. Tarascon, *Nature Mater*., **2009**, 8, 120.
[12] J. A. Kaduk, *Acta Crystallogr.B*, **2000**, 56, 474.
[13] N. Ogihara, T. Yasuda, Y. Kishida, T. Ohsuna, K. Miyamoto, N. Ohba, *Angew. Chem. Int. Ed*. **2014**, 53, 11467.
[14] T. Yasuda, N. Ogihara, *Chem. Commun.* **2014**, 50, 11565.
[15] D. Banerjee, S. J. Kim, J. B. Parise, *Crystal Growth & Design* **2009**, 9, 2500.
[16] S. Wang, L. Wang, K. Zhang, Z. Zhu, Z. Tao, J. Chen, *Nano Lett.*, **2013**, 13, 4404.
[17] B. Häupler, A. Wild, U. S. Schubert, *Adv. Energy Mater.* **2015**, 5, 140234.
[18] P. Ge, M. Fouletier, *Solid State Ionics*, **1988**, 28, 1172.
[19] D. A. Stevens, J. R. Dahn, *J. Electrochem. Soc.*, **2001**, 148, A803.
[20] D. A. Stevens, J. R. Dahn, *J. Electrochem. Soc.*, **2000**, 147, 1271.
[21] L. Zhao, J. Zhao, Y-S. Hu, H. Li, Z. Zhou, M. Armand, L. D. Chen, *Adv. Energy Mater.* **2012**, 2, 962.
[22] A. Abouimrane, W. Weng, H. Eltayeb, Y. Cui, J. Niklas, O. Poluektov, K. Amine, *Energy Environ. Sci.* **2012**, 5, 9632.
[23] Y. Park, D. S. Shin, S. H. Woo, N. S. Choi, K. H. Shin, S. M. Oh, K. T. Lee, S. Y. Hong, *Adv. Mater.* **2012**, 24, 3562.
[24] A. Choi, Y. K. Kim, T. K. Kim, M.-S. Kwon, K. T. Lee, H. R. Moon, *J. Mater. Chem. A*, **2014**, 2, 14986.
[25] S. Wang, L. Wang, Z. Zhu, Z. Hu, Q. Zhao, J. Chen, *Angew. Chem. Int. Ed.* **2014**, 53, 5892.
[26] H. Padhy, Y. Chen, J. Lüder, S.R. Gajella, S. Manzhos, P. Balaya, *Adv. Energy Mater.* **2018**, 8, 1701572.
[27] W. Deng, J. Qian, Y. Cao, X. Ai, H. Yang, *Small* **2016**, 12, 583.
[28] V. Medabalmi, N. Kuanr, K. Ramanujam, *J. Electrochem. Soc.* **2018**, 165**,** A175.
[29] Q. Zhao, Y. Lu, J. Chen, *Adv. Energy Mater.* **2017**, 7**,** 1601792.
[30] A. A. Coelho, *J. Appl. Crystallogr*, **2000**, 33, 899.
[31] A. A. Coelho, J.S.O. Evans, I.R. Evans, A. Kern, S. Parsons, *Powder Diffraction* **2011**, 26, S22.
[32] C.Volkringer, J.Marrot, G.Ferey, T.Loiseau, *Cryst.Growth Des.* **2008**, 8, 685.
[33] K.O.Kongshaug, H.Fjellvag, *J.Solid State Chem.* **2004**, 177, 1852.

[34] S. Cevik, Z. A. Alkaya, H. Dal, Musa Sari, *Synth.React.Inorg.,Met.-Org.,Nano-Met.Chem.* **2016**, 46, 1426.
[35] M. Winter, J. O. Besenhard, M. E. Spahr, P. Novak, *Adv. Mater.* **1998**, 10, 725.
[36] E. Peled, S. Menkin, *J. Electrochem. Soc*. **2017**, 164, A1703.
[37] C. Bommier, X. Ji, *Small* **2018**, 14, 1703576.
[38] B. Philippe, M. Valvo, F. Lindgren, H. Rensmo, K. Edström, *Chem. Mater*. **2014**, 261, 75028.
[39] K. Li, J. Zhang, D. Lin, D.-W. Wang, B. Li, W. Lv, S. Sun, Y.-B. He, F. Kang, Q.-H. Yang, L. Zhou and T. Y. Zhang, *Nature Comm.* **2019**, 10, 725
[40] N. Ogihara, N. Ohba, Y. Kishida, *Sci. Adv.* **2017**, 8, 1603103.
[41] N. Ogihara, Y. Ozawa, O. Hiruta, *J. Mater. Chem. A* **2016**, 4, 3398.
[42]

10.1002/cssc.201901626

WILEY-VCH

Entry for the Table of Contents (Please choose one layout)

Layout 1:

FULL PAPER

Text for Table of Contents

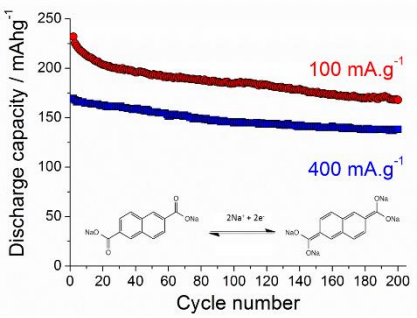

*Joel M. Cabañero Jr, Vanessa Pimenta, Kieran C. Cannon, Russell E. Morris and A. Robert Armstrong**

Page No. – Page No.

Sodium naphthalene-2,6-dicarboxylate: an Anode for Sodium Batteries

Layout 2:

FULL PAPER

((Insert TOC Graphic here; max. width: 11.5 cm; max. height: 2.5 cm))

*Author(s), Corresponding Author(s)**

Page No. – Page No.

Title

Text for Table of Contents